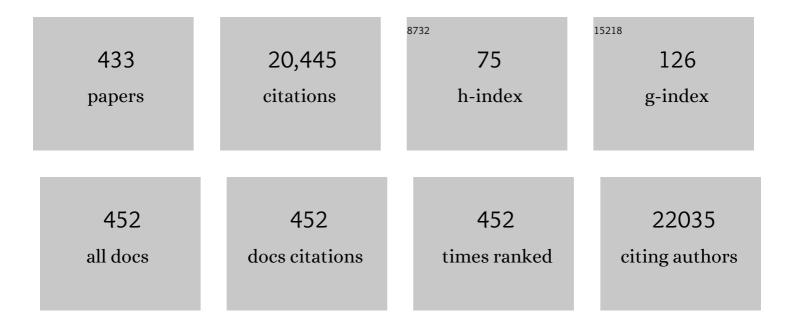
## Martin A Styner

List of Publications by Year in descending order

Source: https://exaly.com/author-pdf/6581423/publications.pdf Version: 2024-02-01



#	Article	IF	CITATIONS
1	A Prospective Evaluation of Infant Cerebellar-Cerebral Functional Connectivity in Relation to Behavioral Development in Autism Spectrum Disorder. Biological Psychiatry Global Open Science, 2023, 3, 149-161.	1.0	3
2	Differential Role for Hippocampal Subfields in Alzheimer's Disease Progression Revealed with Deep Learning. Cerebral Cortex, 2022, 32, 467-478.	1.6	18
3	Hemispheric Cortical, Cerebellar and Caudate Atrophy Associated to Cognitive Impairment in Metropolitan Mexico City Young Adults Exposed to Fine Particulate Matter Air Pollution. Toxics, 2022, 10, 156.	1.6	11
4	Subcortical Brain Development in Autism and Fragile X Syndrome: Evidence for Dynamic, Age- and Disorder-Specific Trajectories in Infancy. American Journal of Psychiatry, 2022, 179, 562-572.	4.0	28
5	Diffusion Tensor Based White Matter Tract Atlases for Pediatric Populations. Frontiers in Neuroscience, 2022, 16, 806268.	1.4	6
6	CONTINUITY: CONnectivity Tool with INtegration of sUbcortical regions, registration and visualization of TractographY. , 2022, , .		0
7	Characterizing the propagation pathway of neuropathological events of Alzheimer's disease using harmonic wavelet analysis. Medical Image Analysis, 2022, 79, 102446.	7.0	2
8	Cerebellar Volumes and Sensorimotor Behavior in Autism Spectrum Disorder. Frontiers in Integrative Neuroscience, 2022, 16, 821109.	1.0	4
9	Relationship of Striatal Presynaptic Dopamine to Midbrain Neuromelanin in a Nonhuman Primate Model of Maternal Immune Activation. Biological Psychiatry, 2022, 91, S60-S61.	0.7	0
10	Infant Visual Brain Development and Inherited Genetic Liability in Autism. American Journal of Psychiatry, 2022, 179, 573-585.	4.0	14
11	TwinEQTL: ultrafast and powerful association analysis for eQTL and GWAS in twin studies. Genetics, 2022, 221, .	1.2	0
12	Impact of gonadectomy on maturational changes in brain volume in adolescent macaques. Psychoneuroendocrinology, 2021, 124, 105068.	1.3	1
13	Learning Common Harmonic Waves on Stiefel Manifold – A New Mathematical Approach for Brain Network Analyses. IEEE Transactions on Medical Imaging, 2021, 40, 419-430.	5.4	14
14	Discovering Spreading Pathways of Neuropathological Events in Alzheimer's Disease Using Harmonic Wavelets. Lecture Notes in Computer Science, 2021, , 228-240.	1.0	1
15	Web infrastructure for data management, storage and computation. , 2021, 11600, .		5
16	Extra axial cerebrospinal fluid volume and a diagnosis of Alzheimer's disease. , 2021, , .		0
17	FlyBy CNN: a 3D surface segmentation framework. , 2021, 11596, .		6
18	Infantile Iron Deficiency Affects Brain Development in Monkeys Even After Treatment of Anemia. Frontiers in Human Neuroscience, 2021, 15, 624107.	1.0	9

#	Article	IF	CITATIONS
19	Placental genomic risk scores and early neurodevelopmental outcomes. Proceedings of the National Academy of Sciences of the United States of America, 2021, 118, .	3.3	25
20	<i>DCC</i> gene network in the prefrontal cortex is associated with total brain volume in childhood. Journal of Psychiatry and Neuroscience, 2021, 46, E154-E163.	1.4	8
21	Robust Cortical Thickness Morphometry of Neonatal Brain and Systematic Evaluation Using Multi-Site MRI Datasets. Frontiers in Neuroscience, 2021, 15, 650082.	1.4	10
22	Structural development of cortical lobes during the first 6 months of life in infant macaques. Developmental Cognitive Neuroscience, 2021, 48, 100906.	1.9	8
23	A Critical Proton MR Spectroscopy Marker of Alzheimer's Disease Early Neurodegenerative Change: Low Hippocampal NAA/Cr Ratio Impacts APOE ε4 Mexico City Children and Their Parents. Advances in Alzheimer's Disease, 2021, , .	0.2	Ο
24	General anaesthesia during infancy reduces white matter micro-organisation in developing rhesus monkeys. British Journal of Anaesthesia, 2021, 126, 845-853.	1.5	17
25	Proteobacteria abundance during nursing predicts physical growth and brain volume at one year of age in young rhesus monkeys. FASEB Journal, 2021, 35, e21682.	0.2	8
26	Clinical decision support systems in orthodontics: A narrative review of data science approaches. Orthodontics and Craniofacial Research, 2021, 24, 26-36.	1.2	16
27	Maternal Immune Activation in Macaques Associated With Alterations in Functional Brain Connectivity. Biological Psychiatry, 2021, 89, S174-S175.	0.7	0
28	The White Matter Connectome as an Early Imaging Biomarker. Biological Psychiatry, 2021, 89, S30.	0.7	1
29	Long-Term Structural Effects of Early Life Stress on Reward and Emotion Regulation Neurocircuitry in Adolescence. Biological Psychiatry, 2021, 89, S275-S276.	0.7	0
30	Infant gut microbiome composition is associated with non-social fear behavior in a pilot study. Nature Communications, 2021, 12, 3294.	5.8	36
31	Genetic Influences on Longitudinal Trajectories of Cortical Thickness and Surface Area during the First 2 Years of Life. Cerebral Cortex, 2021, , .	1.6	3
32	Longitudinal Prediction of Infant MR Images With Multi-Contrast Perceptual Adversarial Learning. Frontiers in Neuroscience, 2021, 15, 653213.	1.4	4
33	Joint hub identification for brain networks by multivariate graph inference. Medical Image Analysis, 2021, 73, 102162.	7.0	4
34	Prospective association of maternal psychosocial stress in pregnancy with newborn hippocampal volume and implications for infant social-emotional development. Neurobiology of Stress, 2021, 15, 100368.	1.9	22
35	Group-wise Hub Identification by Learning Common Graph Embeddings on Grassmannian Manifold. IEEE Transactions on Pattern Analysis and Machine Intelligence, 2021, PP, 1-1.	9.7	0
36	A voxel-wise assessment of growth differences in infants developing autism spectrum disorder. NeuroImage: Clinical, 2021, 29, 102551.	1.4	8

#	Article	IF	CITATIONS
37	Merging and Annotating Teeth and Roots from Automated Segmentation ofÂMultimodal Images. Lecture Notes in Computer Science, 2021, , 81-92.	1.0	4
38	Maternal Immune Activation during Pregnancy Alters Postnatal Brain Growth and Cognitive Development in Nonhuman Primate Offspring. Journal of Neuroscience, 2021, 41, 9971-9987.	1.7	29
39	Automatic Segmentation of Mandibular Ramus and Condyles. , 2021, 2021, 2952-2955.		5
40	Exercise Increases Bone in SEIPIN Deficient Lipodystrophy, Despite Low Marrow Adiposity. Frontiers in Endocrinology, 2021, 12, 782194.	1.5	2
41	Subtyping of mild cognitive impairment using a deep learning model based on brain atrophy patterns. Cell Reports Medicine, 2021, 2, 100467.	3.3	15
42	Automatic Segmentation of Dental Root Canal and Merging with Crown Shape. , 2021, 2021, 2948-2951.		4
43	Influence of Gonadal Steroids on Cortical Surface Area in Infancy. Cerebral Cortex, 2021, , .	1.6	2
44	Exposure to prenatal maternal distress and infant white matter neurodevelopment. Development and Psychopathology, 2021, 33, 1526-1538.	1.4	16
45	Exercise Degrades Bone in Caloric Restriction, Despite Suppression of Marrow Adipose Tissue (MAT). Journal of Bone and Mineral Research, 2020, 35, 106-115.	3.1	23
46	Cortical Structure and Cognition in Infants and Toddlers. Cerebral Cortex, 2020, 30, 786-800.	1.6	25
47	T33. NEUROIMMUNE MECHANISMS OF PSYCHIATRIC DISORDERS: LONGITUDINAL EVALUATION OF DIFFUSION MEASURES OF EXTRACELLULAR FREE WATER IN A NON-HUMAN PRIMATE MODEL OF MATERNAL IMMUNE ACTIVATION. Schizophrenia Bulletin, 2020, 46, S244-S244.	2.3	1
48	M179. ALTERNATED BRAIN AND BEHAVIORAL DEVELOPMENT IN A NONHUMAN PRIMATE MODEL OF MATERNAL IMMUNE ACTIVATION. Schizophrenia Bulletin, 2020, 46, S204-S204.	2.3	0
49	Lexical-semantic search related to side of onset and putamen volume in Parkinson's disease. Brain and Language, 2020, 209, 104841.	0.8	2
50	Individual Variation of Human Cortical Structure Is Established in the First Year of Life. Biological Psychiatry: Cognitive Neuroscience and Neuroimaging, 2020, 5, 971-980.	1.1	11
51	Amygdala Development in Early Childhood: Individual Differences and Associations With Anxiety at Age 4. Biological Psychiatry, 2020, 87, S123-S124.	0.7	0
52	A Novel Method for High-Dimensional Anatomical Mapping of Extra-Axial Cerebrospinal Fluid: Application to the Infant Brain. Frontiers in Neuroscience, 2020, 14, 561556.	1.4	2
53	Neonatal brain volume as a marker of differential susceptibility to parenting quality and its association with neurodevelopment across early childhood. Developmental Cognitive Neuroscience, 2020, 45, 100826.	1.9	9
54	Altered Brain Structure in Infants with Turner Syndrome. Cerebral Cortex, 2020, 30, 587-596.	1.6	15

#	Article	IF	CITATIONS
55	Osteoarthritis of the Temporomandibular Joint can be diagnosed earlier using biomarkers and machine learning. Scientific Reports, 2020, 10, 8012.	1.6	71
56	Sleep Onset Problems and Subcortical Development in Infants Later Diagnosed With Autism Spectrum Disorder. American Journal of Psychiatry, 2020, 177, 518-525.	4.0	52
57	A 3D Fully Convolutional Neural Network With Top-Down Attention-Guided Refinement for Accurate and Robust Automatic Segmentation of Amygdala and Its Subnuclei. Frontiers in Neuroscience, 2020, 14, 260.	1.4	9
58	Characterizing the Propagation Pattern of Neurodegeneration in Alzheimer's Disease by Longitudinal Network Analysis. , 2020, 2020, 292-295.		5
59	White Matter Development from Birth to 6ÂYears of Age: A Longitudinal Study. Cerebral Cortex, 2020, 30, 6152-6168.	1.6	20
60	Personalized connectome fingerprints: Their importance in cognition from childhood to adult years. NeuroImage, 2020, 221, 117122.	2.1	7
61	Neonatal hippocampal volume moderates the effects of early postnatal enrichment on cognitive development. Developmental Cognitive Neuroscience, 2020, 45, 100820.	1.9	12
62	Longitudinal change in autonomic symptoms predicts activities of daily living and depression in Parkinson's disease. Clinical Autonomic Research, 2020, 30, 223-230.	1.4	16
63	Sex differences associated with corpus callosum development in human infants: A longitudinal multimodal imaging study. NeuroImage, 2020, 215, 116821.	2.1	14
64	3D Slicer Craniomaxillofacial Modules Support Patient-Specific Decision-Making for Personalized Healthcare in Dental Research. Lecture Notes in Computer Science, 2020, 12445, 44-53.	1.0	8
65	Patient Specific Classification of Dental Root Canal and Crown Shape. Lecture Notes in Computer Science, 2020, 12474, 145-153.	1.0	9
66	Developmental outcomes of early adverse care on amygdala functional connectivity in nonhuman primates. Development and Psychopathology, 2020, 32, 1579-1596.	1.4	20
67	Long-term alterations in brain and behavior after postnatal Zika virus infection in infant macaques. Nature Communications, 2020, 11, 2534.	5.8	38
68	Alternated Neurodevelopment and Immune Function a Nonhuman Primate Model of Maternal Immune Activation. Biological Psychiatry, 2020, 87, S251.	0.7	0
69	Extra-axial Cerebrospinal Fluid Relationships to Infant Brain Structure, Cognitive Development, and Risk for Schizophrenia. Biological Psychiatry: Cognitive Neuroscience and Neuroimaging, 2020, 5, 651-659.	1.1	9
70	Multi-modal Perceptual Adversarial Learning for Longitudinal Prediction of Infant MR Images. Lecture Notes in Computer Science, 2020, , 284-294.	1.0	1
71	Hierarchical Geodesic Modeling on the Diffusion Orientation Distribution Function for Longitudinal DW-MRI Analysis. Lecture Notes in Computer Science, 2020, 12267, 311-321.	1.0	0
72	A Framework to Construct a Longitudinal DW-MRI Infant Atlas Based on Mixed Effects Modeling of dODF Coefficients. Mathematics and Visualization, 2020, 2020, 149-159.	0.4	2

#	Article	IF	CITATIONS
73	Automatic measurement of extra-axial CSF from infant MRI data. , 2020, 11317, .		1
74	Maternal Cortisol Concentrations During Pregnancy and Sex-Specific Associations With Neonatal Amygdala Connectivity and Emerging Internalizing Behaviors. Biological Psychiatry, 2019, 85, 172-181.	0.7	135
75	Minimally Invasive Approach for Diagnosing TMJ Osteoarthritis. Journal of Dental Research, 2019, 98, 1103-1111.	2.5	45
76	Hierarchical spherical deformation for cortical surface registration. Medical Image Analysis, 2019, 57, 72-88.	7.0	27
77	O53. Maternal Immune Activation Induced Structural Brain Alterations in Macaques: A Longitudinal Study. Biological Psychiatry, 2019, 85, S127.	0.7	0
78	O2.6. A TWO-YEAR LONGITUDINAL EVALUATION OF DIFFUSION MEASURES OF EXTRACELLULAR FREE WATER IN A NON-HUMAN PRIMATE MODEL OF MATERNAL IMMUNE ACTIVATION – EXPLORING NEUROIMMUNE MECHANISMS OF PSYCHIATRIC DISORDERS. Schizophrenia Bulletin, 2019, 45, S164-S165.	2.3	0
79	Individual differences in neonatal white matter are associated with executive function at 3 years of age. Brain Structure and Function, 2019, 224, 3159-3169.	1.2	9
80	T43. Early Emerging Regulatory Behavior Mediates Association Between Newborn Brain Connectivity and Subsequent Internalizing Symptoms. Biological Psychiatry, 2019, 85, S145.	0.7	0
81	T60. The Longitudinal Study of Anesthesia Effects on White Matter Development. Biological Psychiatry, 2019, 85, S151-S152.	0.7	0
82	Role of deep learning in infant brain MRI analysis. Magnetic Resonance Imaging, 2019, 64, 171-189.	1.0	48
83	White matter development in infants at risk for schizophrenia. Schizophrenia Research, 2019, 210, 107-114.	1.1	8
84	3D superimposition of craniofacial imaging—The utility of multicentre collaborations. Orthodontics and Craniofacial Research, 2019, 22, 213-220.	1.2	19
85	White matter connectomes at birth accurately predict cognitive abilities at age 2. NeuroImage, 2019, 192, 145-155.	2.1	47
86	Disentangling the effects of early caregiving experience and heritable factors on brain white matter development in rhesus monkeys. NeuroImage, 2019, 197, 625-642.	2.1	19
87	Transgenic rhesus monkeys carrying the human <i>MCPH1</i> gene copies show human-like neoteny of brain development. National Science Review, 2019, 6, 480-493.	4.6	52
88	F46. Increased Extra-Axial Cerebrospinal Fluid is Associated With Decreased Cortical Thickness and Delayed Motor Development in Early Childhood. Biological Psychiatry, 2019, 85, S230.	0.7	0
89	Neonatal White Matter Maturation Is Associated With Infant Language Development. Frontiers in Human Neuroscience, 2019, 13, 434.	1.0	15
90	F50. Individual Variation of Cortical Morphology at Age 6 is Established in the First Year of Life. Biological Psychiatry, 2019, 85, S231-S232.	0.7	0

#	Article	IF	CITATIONS
91	Association of Prenatal Maternal Depression and Anxiety Symptoms With Infant White Matter Microstructure. Obstetrical and Gynecological Survey, 2019, 74, 138-139.	0.2	0
92	Gut microbiome and brain functional connectivity in infants-a preliminary study focusing on the amygdala. Psychopharmacology, 2019, 236, 1641-1651.	1.5	91
93	Newborn amygdala connectivity and early emerging fear. Developmental Cognitive Neuroscience, 2019, 37, 100604.	1.9	39
94	White matter microstructural development and cognitive ability in the first 2 years of life. Human Brain Mapping, 2019, 40, 1195-1210.	1.9	44
95	Quantitative tractâ€based white matter heritability in 1―and 2â€yearâ€old twins. Human Brain Mapping, 2019, 40, 1164-1173.	1.9	10
96	Restricted and Repetitive Behavior and Brain Functional Connectivity in Infants at Risk for Developing Autism Spectrum Disorder. Biological Psychiatry: Cognitive Neuroscience and Neuroimaging, 2019, 4, 50-61.	1.1	53
97	The UNC/UMN Baby Connectome Project (BCP): An overview of the study design and protocol development. NeuroImage, 2019, 185, 891-905.	2.1	234
98	Environmental Influences on Infant Cortical Thickness and Surface Area. Cerebral Cortex, 2019, 29, 1139-1149.	1.6	60
99	Maternal Interleukin-6 concentration during pregnancy is associated with variation in frontolimbic white matter and cognitive development in early life. NeuroImage, 2019, 185, 825-835.	2.1	150
100	Shape variation analyzer: a classifier for temporomandibular joint damaged by osteoarthritis. , 2019, 10950, .		9
101	Constructing Consistent Longitudinal Brain Networks by Group-Wise Graph Learning. Lecture Notes in Computer Science, 2019, , 654-662.	1.0	2
102	Harmonization and Targeted Feature Dropout for Generalized Segmentation: Application to Multi-site Traumatic Brain Injury Images. Lecture Notes in Computer Science, 2019, , 81-89.	1.0	4
103	Joint Identification of Network Hub Nodes by Multivariate Graph Inference. Lecture Notes in Computer Science, 2019, , 590-598.	1.0	0
104	Semi-supervised VAE-GAN for Out-of-Sample Detection Applied to MRI Quality Control. Lecture Notes in Computer Science, 2019, , 127-136.	1.0	5
105	Hierarchical Multi-geodesic Model for Longitudinal Analysis of Temporal Trajectories of Anatomical Shape and Covariates. Lecture Notes in Computer Science, 2019, , 57-65.	1.0	5
106	Spatiotemporal Modeling for Image Time Series with Appearance Change: Application to Early Brain Development. Lecture Notes in Computer Science, 2019, , 174-185.	1.0	2
107	Model selection for spatiotemporal modeling of early childhood sub-cortical development. , 2019, 10949, .		1
108	Multiseg pipeline: automatic tissue segmentation of brain MR images with subject-specific atlases. , 2019, 10953, .		0

#	Article	IF	CITATIONS
109	Conformal initialization for shape analysis applications in SALT. , 2019, 10953, .		О
110	A web-based system for statistical shape analysis in temporomandibular joint osteoarthritis. , 2019, 10953, .		3
111	Development of White Matter Circuitry in Infants With Fragile X Syndrome. JAMA Psychiatry, 2018, 75, 505.	6.0	35
112	Postnatal Zika virus infection is associated with persistent abnormalities in brain structure, function, and behavior in infant macaques. Science Translational Medicine, 2018, 10, .	5.8	75
113	TRACE: A Topological Graph Representation for Automatic Sulcal Curve Extraction. IEEE Transactions on Medical Imaging, 2018, 37, 1653-1663.	5.4	20
114	A deep neural network to assess spontaneous pain from mouse facial expressions. Molecular Pain, 2018, 14, 174480691876365.	1.0	102
115	Walking, Gross Motor Development, and Brain Functional Connectivity in Infants and Toddlers. Cerebral Cortex, 2018, 28, 750-763.	1.6	65
116	Maternal Systemic Interleukin-6 During Pregnancy Is Associated With Newborn Amygdala Phenotypes and Subsequent Behavior at 2 Years of Age. Biological Psychiatry, 2018, 83, 109-119.	0.7	213
117	Infant Gut Microbiome Associated With CognitiveÂDevelopment. Biological Psychiatry, 2018, 83, 148-159.	0.7	362
118	Intergenerational Effect of Maternal Exposure to Childhood Maltreatment on Newborn Brain Anatomy. Biological Psychiatry, 2018, 83, 120-127.	0.7	138
119	Skeletal Shape Correspondence Through Entropy. IEEE Transactions on Medical Imaging, 2018, 37, 1-11.	5.4	28
120	Computational Texture Features and Mechanical Anisotropy Reflect Structure and Composition of Dystrophic Canine Skeletal Muscle. , 2018, , .		0
121	SlicerSALT: Shape AnaLysis Toolbox. Lecture Notes in Computer Science, 2018, 11167, 65-72.	1.0	20
122	Objective Evaluation of Multiple Sclerosis Lesion Segmentation using a Data Management and Processing Infrastructure. Scientific Reports, 2018, 8, 13650.	1.6	171
123	240. Extracellular Free Water and Glutathione in First Episode Schizophrenia and a Non-Human Primate Model of Maternal Immune Activation – Exploring Neuroimmune Mechanisms of Psychiatric Disorders. Biological Psychiatry, 2018, 83, S97.	0.7	Ο
124	Hierarchical Spherical Deformation for Shape Correspondence. Lecture Notes in Computer Science, 2018, 11070, 853-861.	1.0	0
125	Non-Euclidean, convolutional learning on cortical brain surfaces. , 2018, 2018, 527-530.		3
126	A web-based system for neural network based classification in temporomandibular joint osteoarthritis. Computerized Medical Imaging and Graphics, 2018, 67, 45-54.	3.5	43

#	Article	IF	CITATIONS
127	A cortical shape-adaptive approach to local gyrification index. Medical Image Analysis, 2018, 48, 244-258.	7.0	28
128	Genetic influences on neonatal cortical thickness and surface area. Human Brain Mapping, 2018, 39, 4998-5013.	1.9	43
129	193. Sex Specific Effects of Maternal Cortisol Concentrations During Pregnancy on the Functional Connectivity of the Newborn Limbic System. Biological Psychiatry, 2018, 83, S77-S78.	0.7	1
130	Association of Prenatal Maternal Depression and Anxiety Symptoms With Infant White Matter Microstructure. JAMA Pediatrics, 2018, 172, 973.	3.3	93
131	Exploratory Population Analysis with Unbalanced Optimal Transport. Lecture Notes in Computer Science, 2018, 11072, 464-472.	1.0	4
132	Group-wise shape correspondence of variable and complex objects. , 2018, 10574, .		1
133	TRAFIC: fiber tract classification using deep learning. , 2018, 10574, .		14
134	SVA: shape variation analyzer. , 2018, 10578, .		3
135	A novel framework for the local extraction of extra-axial cerebrospinal fluid from MR brain images. , 2018, 10574, .		2
136	Impact of Demographic and Obstetric Factors on Infant Brain Volumes: A Population Neuroscience Study. Cerebral Cortex, 2017, 27, 5616-5625.	1.6	50
137	Splenium development and early spoken language in human infants. Developmental Science, 2017, 20, e12360.	1.3	36
138	Maternal buffering beyond glucocorticoids: impact of early life stress on corticolimbic circuits that control infant responses to novelty. Social Neuroscience, 2017, 12, 50-64.	0.7	35
139	Joint Attention and Brain Functional Connectivity in Infants and Toddlers. Cerebral Cortex, 2017, 27, 1709-1720.	1.6	103
140	Increased Extra-axial Cerebrospinal Fluid in High-Risk Infants Who Later Develop Autism. Biological Psychiatry, 2017, 82, 186-193.	0.7	173
141	Early brain development in infants at high risk for autism spectrum disorder. Nature, 2017, 542, 348-351.	13.7	808
142	Effects of Antenatal Maternal Depressive Symptoms and Socio-Economic Status on Neonatal Brain Development are Modulated by Genetic Risk. Cerebral Cortex, 2017, 27, 3080-3092.	1.6	90
143	Federating heterogeneous datasets to enhance data sharing and experiment reproducibility. , 2017, 10137, .		3
144	Newborn insula gray matter volume is prospectively associated with early life adiposity gain. International Journal of Obesity, 2017, 41, 1434-1439.	1.6	5

#	Article	IF	CITATIONS
145	Diagnostic index: an open-source tool to classify TMJ OA condyles. , 2017, 10137, .		10
146	742. Gut Microbiome and Brain Functional Connectivity in Infants: A Preliminary Study Focusing on the Amygdala. Biological Psychiatry, 2017, 81, S300-S301.	0.7	1
147	Exercise Decreases Marrow Adipose Tissue Through ß-Oxidation in Obese Running Mice. Journal of Bone and Mineral Research, 2017, 32, 1692-1702.	3.1	78
148	Large deep neural networks for MS lesion segmentation. Proceedings of SPIE, 2017, , .	0.8	0
149	Neural circuitry at age 6Âmonths associated with later repetitive behavior and sensory responsiveness in autism. Molecular Autism, 2017, 8, 8.	2.6	111
150	A segmentation editing framework based on shape change statistics. , 2017, 10133, .		1
151	Functional neuroimaging of high-risk 6-month-old infants predicts a diagnosis of autism at 24 months of age. Science Translational Medicine, 2017, 9, .	5.8	264
152	FADTTSter: accelerating hypothesis testing with functional analysis of diffusion tensor tract statistics. , 2017, 10137, .		2
153	White matter fiber-based analysis of T1w/T2w ratio map. Proceedings of SPIE, 2017, 10133, .	0.8	7
154	The Emergence of Network Inefficiencies in Infants With Autism Spectrum Disorder. Biological Psychiatry, 2017, 82, 176-185.	0.7	93
155	CIVILITY: cloud based interactive visualization of tractography brain connectome. Proceedings of SPIE, 2017, 10137, .	0.8	5
156	A novel maturation index based on neonatal diffusion tensor imaging reflects typical perinatal white matter development in humans. International Journal of Developmental Neuroscience, 2017, 56, 42-51.	0.7	19
157	Common and heritable components of white matter microstructure predict cognitive function at 1 and 2 y. Proceedings of the National Academy of Sciences of the United States of America, 2017, 114, 148-153.	3.3	47
158	Subcortical Brain and Behavior Phenotypes Differentiate Infants With Autism Versus Language Delay. Biological Psychiatry: Cognitive Neuroscience and Neuroimaging, 2017, 2, 664-672.	1.1	71
159	Novel Local Shape-Adaptive Gyrification Index with Application to Brain Development. Lecture Notes in Computer Science, 2017, , 31-39.	1.0	3
160	528. Cognitive Ability is Related to White Matter Tract Integrity in 1-Year-Olds. Biological Psychiatry, 2017, 81, S214.	0.7	0
161	243. Implications of Newborn Amygdala Connectivity on Fear Vs. Negative Emotionality Development over the First Year of Life. Biological Psychiatry, 2017, 81, S100.	0.7	1
162	Genome-wide association analysis identifies common variants influencing infant brain volumes. Translational Psychiatry, 2017, 7, e1188-e1188.	2.4	27

#	Article	IF	CITATIONS
163	Brain structure in sagittal craniosynostosis. , 2017, 10137, .		4
164	Fast predictive multimodal image registration. , 2017, , .		13
165	Quicksilver: Fast predictive image registration – A deep learning approach. NeuroImage, 2017, 158, 378-396.	2.1	444
166	Decreased Axon Caliber Underlies Loss of Fiber Tract Integrity, Disproportional Reductions in White Matter Volume, and Microcephaly in Angelman Syndrome Model Mice. Journal of Neuroscience, 2017, 37, 7347-7361.	1.7	30
167	Cortical gray and subcortical white matter associations in Parkinson's disease. Neurobiology of Aging, 2017, 49, 100-108.	1.5	18
168	The UNC-Wisconsin Rhesus Macaque Neurodevelopment Database: A Structural MRI and DTI Database of Early Postnatal Development. Frontiers in Neuroscience, 2017, 11, 29.	1.4	45
169	Resting-state fMRI in sleeping infants more closely resembles adult sleep than adult wakefulness. PLoS ONE, 2017, 12, e0188122.	1.1	51
170	Conditional Local Distance Correlation for Manifold-Valued Data. Lecture Notes in Computer Science, 2017, 10265, 41-52.	1.0	1
171	Identifying Subnetwork Fingerprints in Structural Connectomes: A Data-Driven Approach. Lecture Notes in Computer Science, 2017, , 79-88.	1.0	2
172	HFPRM: Hierarchical Functional Principal Regression Model for Diffusion Tensor Image Bundle Statistics. Lecture Notes in Computer Science, 2017, 10265, 478-489.	1.0	1
173	Cortical surface shape assessment via sulcal/gyral curve-based gyrification index. , 2016, , .		2
174	Multi-object model-based multi-atlas segmentation for rodent brains using dense discrete correspondences. , 2016, 9784, .		0
175	Enhanced cortical thickness measurements for rodent brains via Lagrangian-based RK4 streamline computation. , 2016, 9784, .		5
176	Registration of Developmental Image Sequences with Missing Data. , 2016, , .		0
177	Autotract: automatic cleaning and tracking of fibers. , 2016, 9784, .		5
178	A framework for incorporating DTI Atlas Builder registration into tract-based spatial statistics and a simulated comparison to standard TBSS. , 2016, 9788, .		2
179	Development of cortical shape in the human brain from 6 to 24months of age via a novel measure of shape complexity. Neurolmage, 2016, 135, 163-176.	2.1	33
180	Entropy-based correspondence improvement of interpolated skeletal models. Computer Vision and Image Understanding, 2016, 151, 72-79.	3.0	4

#	Article	IF	CITATIONS
181	Maternal choline supplementation in a sheep model of first trimester binge alcohol fails to protect against brain volume reductions in peripubertal lambs. Alcohol, 2016, 55, 1-8.	0.8	14
182	Compressive sensing based Q-space resampling for handling fast bulk motion in hardi acquisitions. , 2016, 2016, 907-910.		4
183	Identifying Relationships in Functional and Structural Connectome Data Using aÂHypergraph Learning Method. Lecture Notes in Computer Science, 2016, 9901, 9-17.	1.0	5
184	Dystrophin-deficient dogs with reduced myostatin have unequal muscle growth and greater joint contractures. Skeletal Muscle, 2016, 6, 14.	1.9	22
185	Antenatal depression, treatment with selective serotonin reuptake inhibitors, and neonatal brain structure: A propensity-matched cohort study. Psychiatry Research - Neuroimaging, 2016, 253, 43-53.	0.9	54
186	STGP: Spatio-temporal Gaussian process models for longitudinal neuroimaging data. NeuroImage, 2016, 134, 550-562.	2.1	25
187	Implications of newborn amygdala connectivity for fear and cognitive development at 6-months-of-age. Developmental Cognitive Neuroscience, 2016, 18, 12-25.	1.9	97
188	Non-Euclidean classification of medically imaged objects via s-reps. Medical Image Analysis, 2016, 31, 37-45.	7.0	19
189	Stage-dependent loss of cortical gyrification as Parkinson disease "unfolds― Neurology, 2016, 86, 1143-1151.	1.5	36
190	Entropy-based particle correspondence for shape populations. International Journal of Computer Assisted Radiology and Surgery, 2016, 11, 1221-1232.	1.7	13
191	The pattern of gray matter atrophy in Parkinson's disease differs in cortical and subcortical regions. Journal of Neurology, 2016, 263, 68-75.	1.8	63
192	UNC-Emory Infant Atlases for Macaque Brain Image Analysis: Postnatal Brain Development through 12 Months. Frontiers in Neuroscience, 2016, 10, 617.	1.4	27
193	A Critical Proton MR Spectroscopy Marker of Alzheimer's Disease Early Neurodegenerative Change: Low Hippocampal NAA/Cr Ratio Impacts APOE ɛ4 Mexico City Children and Their Parents. Journal of Alzheimer's Disease, 2015, 48, 1065-1075.	1.2	40
194	VisR ultrasound evaluation of dystrophic muscle degeneration in a dog cross-section and comparison to histology and MRI. , 2015, , .		2
195	The DTI Challenge: Toward Standardized Evaluation of Diffusion Tensor Imaging Tractography for Neurosurgery. Journal of Neuroimaging, 2015, 25, 875-882.	1.0	147
196	Robust estimation of group-wise cortical correspondence with an application to macaque and human neuroimaging studies. Frontiers in Neuroscience, 2015, 9, 210.	1.4	18
197	Evaluation of machine learning algorithms for treatment outcome prediction in patients with epilepsy based on structural connectome data. NeuroImage, 2015, 118, 219-230.	2.1	130
198	Accurate age classification of 6 and 12 month-old infants based on resting-state functional connectivity magnetic resonance imaging data. Developmental Cognitive Neuroscience, 2015, 12, 123-133.	1.9	51

#	Article	IF	CITATIONS
199	Clustering High-Dimensional Landmark-Based Two-Dimensional Shape Data. Journal of the American Statistical Association, 2015, 110, 946-961.	1.8	15
200	LOGISMOS-B for primates: primate cortical surface reconstruction and thickness measurement. , 2015, 9413, .		4
201	Skeletal shape correspondence via entropy minimization. , 2015, 9413, .		3
202	Validation of TMJ osteoarthritis synthetic defect database via non-rigid registration. , 2015, 9417, .		1
203	Neonatal amygdala volume modulates the effects of the early caregiving environment on infant social development. Psychoneuroendocrinology, 2015, 61, 34-35.	1.3	1
204	Automatic sulcal curve extraction on the human cortical surface. , 2015, 9413, .		5
205	Shape index distribution based local surface complexity applied to the human cortex. Proceedings of SPIE, 2015, 9413, .	0.8	2
206	Altered corpus callosum morphology associated with autism over the first 2 years of life. Brain, 2015, 138, 2046-2058.	3.7	169
207	Diagnostic index of three-dimensional osteoarthritic changes in temporomandibular joint condylar morphology. Journal of Medical Imaging, 2015, 2, 1.	0.8	20
208	Automatic tissue segmentation of neonate brain MR Images with subject-specific atlases. Proceedings of SPIE, 2015, 9413, .	0.8	18
209	Quantitative tract-based white matter heritability in twin neonates. NeuroImage, 2015, 111, 123-135.	2.1	43
210	Incorporating 3-dimensional models in online articles. American Journal of Orthodontics and Dentofacial Orthopedics, 2015, 147, S195-S204.	0.8	34
211	Diagnostic index of 3D osteoarthritic changes in TMJ condylar morphology. , 2015, 9414, .		8
212	Early postnatal myelin content estimate of white matter via T1w/T2w ratio. , 2015, 9417, .		19
213	Exercise Regulation of Marrow Fat in the Setting of PPARÎ <sup>3</sup> Agonist Treatment in Female C57BL/6 Mice. Endocrinology, 2015, 156, 2753-2761.	1.4	52
214	Fitting Skeletal Object Models Using Spherical Harmonics Based Template Warping. IEEE Signal Processing Letters, 2015, 22, 2269-2273.	2.1	4
215	A diffusion tensor MRI atlas of the postmortem rhesus macaque brain. NeuroImage, 2015, 117, 408-416.	2.1	169
216	Regional differences in fiber tractography predict neurodevelopmental outcomes in neonates with infantile Krabbe disease. NeuroImage: Clinical, 2015, 7, 792-798.	1.4	25

#	Article	IF	CITATIONS
217	Effects of prenatal cocaine exposure on early postnatal rodent brain structure and diffusion properties. Neurotoxicology and Teratology, 2015, 47, 80-88.	1.2	10
218	Shape Abnormalities of the Caudate Nucleus Correlate with Poorer Gait and Balance: Results from a Subset of the LADIS Study. American Journal of Geriatric Psychiatry, 2015, 23, 59-71.e1.	0.6	16
219	Kronecker Product Linear Exponent AR(1) Correlation Structures for Multivariate Repeated Measures. PLoS ONE, 2014, 9, e88864.	1.1	9
220	UNC-Utah NA-MIC framework for DTI fiber tract analysis. Frontiers in Neuroinformatics, 2014, 7, 51.	1.3	54
221	DTIPrep: quality control of diffusion-weighted images. Frontiers in Neuroinformatics, 2014, 8, 4.	1.3	221
222	Multi-atlas segmentation of subcortical brain structures via the AutoSeg software pipeline. Frontiers in Neuroinformatics, 2014, 8, 7.	1.3	98
223	A joint framework for 4D segmentation and estimation of smooth temporal appearance changes. , 2014, 2014, 1291-1294.		2
224	Multi-atlas segmentation with particle-based group-wise image registration. , 2014, 9034, 903447.		4
225	A preliminary study on the effect of motion correction on HARDI reconstruction. , 2014, 2014, 1055-1058.		4
226	Separability tests for high-dimensional, low-sample size multivariate repeated measures data. Journal of Applied Statistics, 2014, 41, 2450-2461.	0.6	9
227	Parametric regression scheme for distributions: Analysis of DTI fiber tract diffusion changes in early brain development. , 2014, 2014, 559-562.		1
228	The Australian, US, Scandinavian Imaging Exchange (AUSSIE): an innovative, virtually-integrated health research network embedded in health care. Australasian Psychiatry, 2014, 22, 260-265.	0.4	4
229	Early adverse experience increases emotional reactivity in juvenile rhesus macaques: Relation to amygdala volume. Developmental Psychobiology, 2014, 56, 1735-1746.	0.9	48
230	Subjectââ,¬â€œMotion Correction in HARDI Acquisitions: Choices and Consequences. Frontiers in Neurology, 2014, 5, 240.	1.1	12
231	NBD delivery improves the disease phenotype of the golden retriever model of Duchenne muscular dystrophy. Skeletal Muscle, 2014, 4, 18.	1.9	30
232	Common Variants in Psychiatric Risk Genes Predict Brain Structure at Birth. Cerebral Cortex, 2014, 24, 1230-1246.	1.6	125
233	Population variation in neuroendocrine activity is associated with behavioral inhibition and hemispheric brain structure in young rhesus monkeys. Psychoneuroendocrinology, 2014, 47, 56-67.	1.3	8
234	SGPP: spatial Gaussian predictive process models for neuroimaging data. NeuroImage, 2014, 89, 70-80.	2.1	19

#	Article	IF	CITATIONS
235	FMEM: Functional mixed effects modeling for the analysis of longitudinal white matter Tract data. NeuroImage, 2014, 84, 753-764.	2.1	23
236	Dysmorphogenic Effects of First Trimester-Equivalent Ethanol Exposure in Mice: A Magnetic Resonance Microscopy-Based Study. Alcoholism: Clinical and Experimental Research, 2014, 38, 2008-2014.	1.4	38
237	3D osteoarthritic changes in TMJ condylar morphology correlates with specific systemic and local biomarkers of disease. Osteoarthritis and Cartilage, 2014, 22, 1657-1667.	0.6	80
238	Adolescent binge ethanol treatment alters adult brain regional volumes, cortical extracellular matrix protein and behavioral flexibility. Pharmacology Biochemistry and Behavior, 2014, 116, 142-151.	1.3	147
239	Impact of Sex and Gonadal Steroids on Neonatal Brain Structure. Cerebral Cortex, 2014, 24, 2721-2731.	1.6	88
240	Bone marrow fat accumulation accelerated by high fat diet is suppressed by exercise. Bone, 2014, 64, 39-46.	1.4	124
241	Characteristics of magnetic resonance imaging biomarkers in a natural history study of golden retriever muscular dystrophy. Neuromuscular Disorders, 2014, 24, 178-191.	0.3	46
242	Investigating the tradeoffs between spatial resolution and diffusion sampling for brain mapping with diffusion tractography: Time well spent?. Human Brain Mapping, 2014, 35, 5667-5685.	1.9	36
243	Multivariate Longitudinal Shape Analysis of Human Lateral Ventricles during the First Twenty-Four Months of Life. PLoS ONE, 2014, 9, e108306.	1.1	9
244	Diffusion imaging quality control via entropy of principal direction distribution. NeuroImage, 2013, 82, 1-12.	2.1	18
245	A computerized MRI biomarker quantification scheme for a canine model of Duchenne muscular dystrophy. International Journal of Computer Assisted Radiology and Surgery, 2013, 8, 763-774.	1.7	31
246	Magnetic resonance microscopy-based analyses of the neuroanatomical effects of gestational day 9 ethanol exposure in mice. Neurotoxicology and Teratology, 2013, 39, 77-83.	1.2	45
247	Alteration to hippocampal shape in cannabis users with and without schizophrenia. Schizophrenia Research, 2013, 143, 179-184.	1.1	54
248	Longitudinal Image Registration With Temporally-Dependent Image Similarity Measure. IEEE Transactions on Medical Imaging, 2013, 32, 1939-1951.	5.4	14
249	Localized differences in caudate and hippocampal shape are associated with schizophrenia but not antipsychotic type. Psychiatry Research - Neuroimaging, 2013, 211, 1-10.	0.9	23
250	Striatal shape in Parkinson's disease. Neurobiology of Aging, 2013, 34, 2510-2516.	1.5	60
251	Cortical correspondence via sulcal curve-constrained spherical registration with application to Macaque studies. , 2013, 8669, .		5
252	Imaging Patients with Psychosis and a Mouse Model Establishes a Spreading Pattern of Hippocampal Dysfunction and Implicates Glutamate as a Driver. Neuron, 2013, 78, 81-93.	3.8	483

#	Article	IF	CITATIONS
253	Multiscale adaptive generalized estimating equations for longitudinal neuroimaging data. NeuroImage, 2013, 72, 91-105.	2.1	32
254	Adaptive prior probability and spatial temporal intensity change estimation for segmentation of the one-year-old human brain. Journal of Neuroscience Methods, 2013, 212, 43-55.	1.3	29
255	Associations between white matter microstructure and infants' working memory. NeuroImage, 2013, 64, 156-166.	2.1	90
256	Software-based diffusion MR human brain phantom for evaluating fiber-tracking algorithms. , 2013, 8669, .		3
257	UNC-Utah NA-MIC DTI framework: atlas based fiber tract analysis with application to a study of nicotine smoking addiction. Proceedings of SPIE, 2013, 8669, .	0.8	3
258	Fiber feature map based landmark initialization for highly deformable DTI registration. , 2013, 8669, .		1
259	3D of brain shape and volume after cranial vault remodeling surgery for craniosynostosis correction in infants. , 2013, 8672, 86720V.		8
260	Statistical texture analysis based MRI quantification of Duchenne muscular dystrophy in a canine model. Proceedings of SPIE, 2013, , .	0.8	7
261	DTI quality control assessment via error estimation from Monte Carlo simulations. Proceedings of SPIE, 2013, 8669, 1667549.	0.8	5
262	White Matter Microstructure and Atypical Visual Orienting in 7-Month-Olds at Risk for Autism. American Journal of Psychiatry, 2013, 170, 899-908.	4.0	228
263	Lateral ventricle morphology analysis via mean latitude axis. , 2013, 8672, .		12
264	Diffusion Tensor Imaging–Based Characterization of Brain Neurodevelopment in Primates. Cerebral Cortex, 2013, 23, 36-48.	1.6	49
265	Spatiotemporal modeling of distribution-valued data applied to DTI tract evolution in infant neurodevelopment. , 2013, 2013, 684-687.		2
266	Frontolimbic neural circuitry at 6Âmonths predicts individual differences in joint attention at 9Âmonths. Developmental Science, 2013, 16, 186-197.	1.3	77
267	Varying coefficient model for modeling diffusion tensors along white matter tracts. Annals of Applied Statistics, 2013, 7, 102-125.	0.5	8
268	A midas plugin to enable construction of reproducible web-based image processing pipelines. Frontiers in Neuroinformatics, 2013, 7, 46.	1.3	0
269	Group-Wise Cortical Correspondence via Sulcal Curve-Constrained Entropy Minimization. Lecture Notes in Computer Science, 2013, 23, 364-375.	1.0	9
270	Particle-Guided Image Registration. Lecture Notes in Computer Science, 2013, 16, 203-210.	1.0	4

#	Article	IF	CITATIONS
271	Geodesic Distances to Landmarks for Dense Correspondence on Ensembles of Complex Shapes. Lecture Notes in Computer Science, 2013, 16, 19-26.	1.0	14
272	A Longitudinal Functional Analysis Framework for Analysis of White Matter Tract Statistics. Lecture Notes in Computer Science, 2013, 23, 220-231.	1.0	5
273	Combined SPHARM-PDM and entropy-based particle systems shape analysis framework. , 2012, 8317, 8317OL.		10
274	Differences in White Matter Fiber Tract Development Present From 6 to 24 Months in Infants With Autism. American Journal of Psychiatry, 2012, 169, 589-600.	4.0	555
275	Brain Volume Findings in 6-Month-Old Infants at High Familial Risk for Autism. American Journal of Psychiatry, 2012, 169, 601-608.	4.0	83
276	Size and shape of the caudate nucleus in individuals with bipolar affective disorder. Australian and New Zealand Journal of Psychiatry, 2012, 46, 340-351.	1.3	37
277	Longitudinal Development of Cortical and Subcortical Gray Matter from Birth to 2 Years. Cerebral Cortex, 2012, 22, 2478-2485.	1.6	377
278	White Matter Heritability Using Diffusion Tensor Imaging in Neonatal Brains. Twin Research and Human Genetics, 2012, 15, 336-350.	0.3	44
279	Automatic corpus callosum segmentation using a deformable active Fourier contour model. , 2012, 8317, .		16
280	White Matter Hyperintensities, Systemic Inflammation, Brain Growth, and Cognitive Functions in Children Exposed to Air Pollution. Journal of Alzheimer's Disease, 2012, 31, 183-191.	1.2	95
281	3D Tensor Normalization for Improved Accuracy in DTI Tensor Registration Methods. Lecture Notes in Computer Science, 2012, , 170-179.	1.0	0
282	Trajectories of Early Brain Volume Development in Fragile X Syndrome and Autism. Journal of the American Academy of Child and Adolescent Psychiatry, 2012, 51, 921-933.	0.3	86
283	Intrinsic Regression Models for Medial Representation of Subcortical Structures. Journal of the American Statistical Association, 2012, 107, 12-23.	1.8	5
284	Multi-contrast diffusion tensor image registration with structural MRI. , 2012, , .		3
285	Prenatal isolated mild ventriculomegaly is associated with persistent ventricle enlargement at ages 1 and 2. Early Human Development, 2012, 88, 691-698.	0.8	38
286	Imaging nigral pathology and clinical progression in Parkinson's disease. Movement Disorders, 2012, 27, 1636-1643.	2.2	107
287	Postnatal day 7 ethanol treatment causes persistent reductions in adult mouse brain volume and cortical neurons with sex specific effects on neurogenesis. Alcohol, 2012, 46, 603-612.	0.8	52
288	Asymmetric bias in user guided segmentations of brain structures. NeuroImage, 2012, 59, 1315-1323.	2.1	47

#	Article	IF	CITATIONS
289	Quantitative tract-based white matter development from birth to age 2 years. Neurolmage, 2012, 61, 542-557.	2.1	179
290	Semiparametric Bayesian local functional models for diffusion tensor tract statistics. NeuroImage, 2012, 63, 460-474.	2.1	3
291	The Paradox of Muscle Hypertrophy in Muscular Dystrophy. Physical Medicine and Rehabilitation Clinics of North America, 2012, 23, 149-172.	0.7	85
292	Hippocampal Shape and Volume Changes with Antipsychotics in Early Stage Psychotic Illness. Frontiers in Psychiatry, 2012, 3, 96.	1.3	42
293	Hippocampal Shape Analysis in Alzheimer's Disease and Frontotemporal Lobar Degeneration Subtypes. Journal of Alzheimer's Disease, 2012, 30, 355-365.	1.2	94
294	The Translational Role of Diffusion Tensor Image Analysis in Animal Models of Developmental Pathologies. Developmental Neuroscience, 2012, 34, 5-19.	1.0	21
295	Projection Regression Models for Multivariate Imaging Phenotype. Genetic Epidemiology, 2012, 36, 631-641.	0.6	15
296	TWO ANATOMIC RESOURCES OF CANINE PELVIC LIMB MUSCLES BASED ON CT AND MRI. Veterinary Radiology and Ultrasound, 2012, 53, n/a-n/a.	0.4	4
297	TwinMARM: Two-Stage Multiscale Adaptive Regression Methods for Twin Neuroimaging Data. IEEE Transactions on Medical Imaging, 2012, 31, 1100-1112.	5.4	15
298	Canine models of Duchenne muscular dystrophy and their use in therapeutic strategies. Mammalian Genome, 2012, 23, 85-108.	1.0	140
299	Pre-organizing Shape Instances for Landmark-Based Shape Correspondence. International Journal of Computer Vision, 2012, 97, 210-228.	10.9	11
300	Metamorphic Geodesic Regression. Lecture Notes in Computer Science, 2012, 15, 197-205.	1.0	19
301	Ethanol-Induced Face-Brain Dysmorphology Patterns Are Correlative and Exposure-Stage Dependent. PLoS ONE, 2012, 7, e43067.	1.1	122
302	Temporally-Dependent Image Similarity Measure for Longitudinal Analysis. Lecture Notes in Computer Science, 2012, , 99-109.	1.0	2
303	Longitudinal Image Registration with Non-uniform Appearance Change. Lecture Notes in Computer Science, 2012, 15, 280-288.	1.0	3
304	Clinical Application of 3D Imaging for Assessment of Treatment Outcomes. Seminars in Orthodontics, 2011, 17, 72-80.	0.8	58
305	Group-wise automatic mesh-based analysis of cortical thickness. , 2011, , .		7
306	DTI registration in atlas based fiber analysis of infantile Krabbe disease. NeuroImage, 2011, 55, 1577-1586.	2.1	110

#	Article	IF	CITATIONS
307	FADTTS: Functional analysis of diffusion tensor tract statistics. NeuroImage, 2011, 56, 1412-1425.	2.1	66
308	Exposure to severe urban air pollution influences cognitive outcomes, brain volume and systemic inflammation in clinically healthy children. Brain and Cognition, 2011, 77, 345-355.	0.8	256
309	Brain enlargement and increased behavioral and cytokine reactivity in infant monkeys following acute prenatal endotoxemia. Behavioural Brain Research, 2011, 219, 108-115.	1.2	79
310	Soft tissue response to mandibular advancement using 3D CBCT scanning. International Journal of Oral and Maxillofacial Surgery, 2011, 40, 353-359.	0.7	51
311	Three-dimensional quantification of mandibular asymmetry through cone-beam computerized tomography. Oral Surgery Oral Medicine Oral Pathology Oral Radiology and Endodontics, 2011, 111, 757-770.	1.6	63
312	Use of High Resolution 3D Diffusion Tensor Imaging to Study Brain White Matter Development in Live Neonatal Rats. Frontiers in Psychiatry, 2011, 2, 54.	1.3	10
313	Two-stage empirical likelihood for longitudinal neuroimaging data. Annals of Applied Statistics, 2011, 5, 1132-1158.	0.5	7
314	Adolescent Binge Drinking Alters Adult Brain Neurotransmitter Gene Expression, Behavior, Brain Regional Volumes, and Neurochemistry in Mice. Alcoholism: Clinical and Experimental Research, 2011, 35, 671-688.	1.4	174
315	Shape analysis of the neostriatum in subtypes of frontotemporal lobar degeneration: Neuroanatomically significant regional morphologic change. Psychiatry Research - Neuroimaging, 2011, 191, 98-111.	0.9	21
316	Shape alterations in the striatum in chorea-acanthocytosis. Psychiatry Research - Neuroimaging, 2011, 192, 29-36.	0.9	49
317	Morphometric analysis of subcortical structures in progressive supranuclear palsy: In vivo evidence of neostriatal and mesencephalic atrophy. Psychiatry Research - Neuroimaging, 2011, 194, 163-175.	0.9	37
318	Steady and Oscillatory Fluid Flows Produce a Similar Osteogenic Phenotype. Calcified Tissue International, 2011, 88, 189-197.	1.5	38
319	Outcome quantification using SPHARM-PDM toolbox in orthognathic surgery. International Journal of Computer Assisted Radiology and Surgery, 2011, 6, 617-626.	1.7	38
320	Combined R2* and Diffusion Tensor Imaging Changes in the Substantia Nigra in Parkinson's Disease. Movement Disorders, 2011, 26, 1627-1632.	2.2	163
321	Clinical application of SPHARM-PDM to quantify temporomandibular joint osteoarthritis. Computerized Medical Imaging and Graphics, 2011, 35, 345-352.	3.5	53
322	Information Filtering for Ultrasound-Based Real-Time Registration. IEEE Transactions on Biomedical Engineering, 2011, 58, 531-540.	2.5	13
323	Automatic skull-stripping of rat MRI/DTI scans and atlas building. , 2011, 7962, 7962251-7962257.		19
324	Twin-Singleton Differences in Neonatal Brain Structure. Twin Research and Human Genetics, 2011, 14, 268-276.	0.3	20

#	Article	IF	CITATIONS
325	Using tensor-based morphometry to detect structural brain abnormalities in rats with adolescent intermittent alcohol exposure. , 2011, , .		0
326	Smaller Brain Volumes and Subtle Cognitive Decline in Overweight Healthy Older Adults. Medicine and Science in Sports and Exercise, 2011, 43, 127.	0.2	1
327	Efficient, graph-based white matter connectivity from orientation distribution functions via multi-directional graph propagation. , 2011, 7962, 79620S.		1
328	MRI-based quantification of Duchenne muscular dystrophy in a canine model. , 2011, , .		4
329	Automatic cortical thickness analysis on rodent brain. , 2011, 7962, 7962481-79624811.		14
330	Mandibular asymmetry characterization using generalized tensor-based morphometry. , 2011, 2011, 1175-1178.		3
331	Spatial intensity prior correction for tissue segmentation in the developing human brain. , $2011$ , , $2049$ -2052.		2
332	Early Brain Overgrowth in Autism Associated With an Increase in Cortical Surface Area Before Age 2 Years. Archives of General Psychiatry, 2011, 68, 467.	13.8	384
333	Geometric Correspondence for Ensembles of Nonregular Shapes. Lecture Notes in Computer Science, 2011, 14, 368-375.	1.0	12
334	Atlas-Guided Segmentation of Vervet Monkey Brain MRI. Open Neuroimaging Journal, 2011, 5, 186-197.	0.2	14
335	Two-Stage Multiscale Adaptive Regression Methods for Twin Neuroimaging Data. Lecture Notes in Computer Science, 2011, , 102-109.	1.0	0
336	Cranial base superimposition for 3-dimensional evaluation of soft-tissue changes. American Journal of Orthodontics and Dentofacial Orthopedics, 2010, 137, S120-S129.	0.8	92
337	Three-dimensional surgical simulation. American Journal of Orthodontics and Dentofacial Orthopedics, 2010, 138, 361-371.	0.8	112
338	FRATS: Functional Regression Analysis of DTI Tract Statistics. IEEE Transactions on Medical Imaging, 2010, 29, 1039-1049.	5.4	33
339	Comparison of Actual Surgical Outcomes and 3-Dimensional Surgical Simulations. Journal of Oral and Maxillofacial Surgery, 2010, 68, 2412-2421.	0.5	144
340	Genetic and environmental contributions to neonatal brain structure: A twin study. Human Brain Mapping, 2010, 31, 1174-1182.	1.9	115
341	Magnetic resonance microscopyâ€based analyses of the brains of normal and ethanolâ€exposed fetal mice. Birth Defects Research Part A: Clinical and Molecular Teratology, 2010, 88, 953-964.	1.6	56
342	A linear exponent AR(1) family of correlation structures. Statistics in Medicine, 2010, 29, 1825-1838.	0.8	28

#	Article	IF	CITATIONS
343	Magnetic Resonance Microscopy Defines Ethanolâ€Induced Brain Abnormalities in Prenatal Mice: Effects of Acute Insult on Gestational Day 7. Alcoholism: Clinical and Experimental Research, 2010, 34, 98-111.	1.4	113
344	Correlation of Automated Volumetric Analysis of Brain MR Imaging with Cognitive Impairment in a Natural History Study of Mucopolysaccharidosis II. American Journal of Neuroradiology, 2010, 31, 1319-1323.	1.2	34
345	Accuracy and Landmark Error Calculation Using Cone-Beam Computed Tomography–Generated Cephalograms. Angle Orthodontist, 2010, 80, 286-294.	1.1	47
346	Quality control of diffusion weighted images. Proceedings of SPIE, 2010, 7628, .	0.8	123
347	Automatic bone segmentation and alignment from MR knee images. Proceedings of SPIE, 2010, , .	0.8	4
348	Changes of MR and DTI appearance in early human brain development. Proceedings of SPIE, 2010, 7623, .	0.8	2
349	Evaluation of DTI property maps as basis of DTI atlas building. , 2010, 7623, .		3
350	Prenatal and Neonatal Brain Structure and White Matter Maturation in Children at High Risk for Schizophrenia. American Journal of Psychiatry, 2010, 167, 1083-1091.	4.0	88
351	Maturational Trajectories of Cortical Brain Development through the Pubertal Transition: Unique Species and Sex Differences in the Monkey Revealed through Structural Magnetic Resonance Imaging. Cerebral Cortex, 2010, 20, 1053-1063.	1.6	92
352	Maternal Influenza Infection During Pregnancy Impacts Postnatal Brain Development in the Rhesus Monkey. Biological Psychiatry, 2010, 67, 965-973.	0.7	161
353	Shape analysis of the neostriatum in frontotemporal lobar degeneration, Alzheimer's disease, and controls. NeuroImage, 2010, 51, 970-986.	2.1	24
354	Three-Dimensional Superimposition for Quantification of Treatment Outcomes. , 2010, , 36-44.		2
355	Multi-Object Analysis of Volume, Pose, and Shape Using Statistical Discrimination. IEEE Transactions on Pattern Analysis and Machine Intelligence, 2010, 32, 652-661.	9.7	49
356	Multivariate Varying Coefficient Models for DTI Tract Statistics. Lecture Notes in Computer Science, 2010, 13, 690-697.	1.0	7
357	DTI Connectivity by Segmentation. Lecture Notes in Computer Science, 2010, , 200-210.	1.0	1
358	Voxel-wise group analysis of DTI. , 2009, , 807-810.		17
359	Diffusion Tensor Imaging Detects Abnormalities in the Corticospinal Tracts of Neonates with Infantile Krabbe Disease. American Journal of Neuroradiology, 2009, 30, 1017-1021.	1.2	60

Evaluation of atlas based mouse brain segmentation. , 2009, 7259, 725943-725949.

21

#	Article	IF	CITATIONS
361	Comparison and Evaluation of Methods for Liver Segmentation From CT Datasets. IEEE Transactions on Medical Imaging, 2009, 28, 1251-1265.	5.4	848
362	Adjusted Exponentially Tilted Likelihood with Applications to Brain Morphology. Biometrics, 2009, 65, 919-927.	0.8	9
363	Magnetic Resonance Microscopy Defines Ethanolâ€Induced Brain Abnormalities in Prenatal Mice: Effects of Acute Insult on Gestational Day 8. Alcoholism: Clinical and Experimental Research, 2009, 33, 1001-1011.	1.4	127
364	Asymmetrical lateral ventricular enlargement in Parkinson's disease. European Journal of Neurology, 2009, 16, 475-481.	1.7	49
365	Standardized evaluation methodology and reference database for evaluating coronary artery centerline extraction algorithms. Medical Image Analysis, 2009, 13, 701-714.	7.0	295
366	Pharyngeal airway volume and shape from cone-beam computed tomography: Relationship to facial morphology. American Journal of Orthodontics and Dentofacial Orthopedics, 2009, 136, 805-814.	0.8	206
367	Shape abnormalities of caudate nucleus in schizotypal personality disorder. Schizophrenia Research, 2009, 110, 127-139.	1.1	32
368	A comparison of automated segmentation and manual tracing for quantifying hippocampal and amygdala volumes. NeuroImage, 2009, 45, 855-866.	2.1	482
369	Rebuttal to Hasan and Pedraza in comments and controversies: "Improving the reliability of manual and automated methods for hippocampal and amygdala volume measurements― NeuroImage, 2009, 48, 499-500.	2.1	7
370	Cortical Correspondence with Probabilistic Fiber Connectivity. Lecture Notes in Computer Science, 2009, 21, 651-663.	1.0	20
371	Intrinsic Regression Models for Manifold-Valued Data. Lecture Notes in Computer Science, 2009, 5762, 192-199.	1.0	27
372	Intrinsic regression models for manifold-valued data. , 2009, 12, 192-9.		3
373	CONDYLAR RESORPTION IN PATIENTS WITH TMD. Craniofacial Growth Series, 2009, 46, 147-157.	0.0	2
374	Local Shape Analysis using MANCOVA. The Insight Journal, 2009, , .	0.2	8
375	A method for frame-by-frame us to CT registration in a joint calibration and registration framework. , 2008, , .		5
376	Multivariate nonlinear mixed model to analyze longitudinal image data: MRI study of early brain development. , 2008, , .		3
377	Functional Connectivity MR Imaging Reveals Cortical Functional Connectivity in the Developing Brain. American Journal of Neuroradiology, 2008, 29, 1883-1889.	1.2	194
378	Minimum description length with local geometry. , 2008, , .		7

Minimum description length with local geometry. , 2008, , . 378

#	Article	IF	CITATIONS
379	Cortical correspondence using entropy-based particle systems and local features. , 2008, , .		23
380	Multivariate longitudinal statistics for neonatal-pediatric brain tissue development. Proceedings of SPIE, 2008, , .	0.8	2
381	Automatic regional analysis of DTI properties in the developmental macaque brain. Proceedings of SPIE, 2008, , .	0.8	4
382	Hippocampus Shape Analysis and Late-Life Depression. PLoS ONE, 2008, 3, e1837.	1.1	77
383	Kalman Filtering for Frame-by-Frame CT to Ultrasound Rigid Registration. Lecture Notes in Computer Science, 2008, , 185-192.	1.0	3
384	Particle-Based Shape Analysis of Multi-object Complexes. Lecture Notes in Computer Science, 2008, 11, 477-485.	1.0	33
385	Assessment of Reliability of Multi-site Neuroimaging Via Traveling Phantom Study. Lecture Notes in Computer Science, 2008, 11, 263-270.	1.0	28
386	Impact of Aerobic Fitness on Cerebral White Matter Integrity in the Cingulum Medicine and Science in Sports and Exercise, 2008, 40, S299-S300.	0.2	1
387	Automatic brain segmentation in rhesus monkeys. , 2007, 6512, 883.		20
388	ROI constrained statistical surface morphometry. , 2007, , .		3
389	CORRESPONDENCE EVALUATION IN LOCAL SHAPE ANALYSIS AND STRUCTURAL SUBDIVISION. , 2007, , .		12
390	Statistical Shape Analysis of Multi-Object Complexes. , 2007, , .		19
391	DYNAMIC REGISTRATION USING ULTRASOUND FOR ANATOMICAL REFERENCING. , 2007, , .		3
392	Statistical group differences in anatomical shape analysis using Hotelling T2 metric. , 2007, , .		6
393	Subcortical structure segmentation using probabilistic atlas priors. , 2007, , .		36
394	Asymmetric bias in user guided segmentations of brain structures. , 2007, , .		1
395	Discrimination analysis using multi-object statistics of shape and pose. , 2007, , .		3
396	Asymmetrical ventricular enlargement in Parkinson's disease. Movement Disorders, 2007, 22, 1657-1660.	2.2	11

#	Article	IF	CITATIONS
397	Accurate and Robust Reconstruction of a Surface Model of the Proximal Femur From Sparse-Point Data and a Dense-Point Distribution Model for Surgical Navigation. IEEE Transactions on Biomedical Engineering, 2007, 54, 2109-2122.	2.5	45
398	Three-dimensional cone-beam computed tomography for assessment of mandibular changes after orthognathic surgery. American Journal of Orthodontics and Dentofacial Orthopedics, 2007, 131, 44-50.	0.8	172
399	Statistical deformable bone models for robust 3D surface extrapolation from sparse data. Medical Image Analysis, 2007, 11, 99-109.	7.0	102
400	Shape Modeling and Analysis with Entropy-Based Particle Systems. Lecture Notes in Computer Science, 2007, 20, 333-345.	1.0	118
401	Assessing the feasibility of ultrasound-initialized deformable bone models. , 2006, , .		3
402	Reduced Relationship to Cortical White Matter Volume Revealed by Tractography-Based Segmentation of the Corpus Callosum in Young Children With Developmental Delay. American Journal of Psychiatry, 2006, 163, 2157-2163.	4.0	22
403	Image analysis and superimposition of 3-dimensional cone-beam computed tomography models. American Journal of Orthodontics and Dentofacial Orthopedics, 2006, 129, 611-618.	0.8	274
404	Computer-assisted arthroplasty using bioengineered autografts. IEEE Engineering in Medicine and Biology Magazine, 2006, 25, 63-69.	1.1	1
405	Reconstruction of Patient-Specific 3D Bone Surface from 2D Calibrated Fluoroscopic Images and Point Distribution Model. Lecture Notes in Computer Science, 2006, 9, 25-32.	1.0	43
406	Statistics of Pose and Shape in Multi-object Complexes Using Principal Geodesic Analysis. Lecture Notes in Computer Science, 2006, , 1-8.	1.0	10
407	Framework for the Statistical Shape Analysis of Brain Structures using SPHARM-PDM. The Insight Journal, 2006, , 242-250.	0.2	154
408	Implementing the Automatic Generation of 3D Statistical Shape Models with ITK. The Insight Journal, 2006, , .	0.2	10
409	KWMeshVisu: A Mesh Visualization Tool for Shape Analysis. The Insight Journal, 2006, , .	0.2	3
410	Framework for the Statistical Shape Analysis of Brain Structures using SPHARM-PDM. The Insight Journal, 2006, , .	0.2	107
411	A novel and stable approach to anatomical structure morphing for enhanced intraoperative 3D visualization. , 2005, , .		17
412	Superimposition of 3D cone-beam CT models of orthognathic surgery patients. Dentomaxillofacial Radiology, 2005, 34, 369-375.	1.3	281
413	Kernel Regularized Bone Surface Reconstruction from Partial Data Using Statistical Shape Model. , 2005, 2005, 6579-82.		2
414	Morphometric analysis of lateral ventricles in schizophrenia and healthy controls regarding genetic and disease-specific factors. Proceedings of the National Academy of Sciences of the United States of America, 2005, 102, 4872-4877.	3.3	146

#	Article	IF	CITATIONS
415	A comparison study assessing the feasibility of ultrasound-initialized deformable bone models. Computer Aided Surgery, 2005, 10, 293-299.	1.8	13
416	Evaluation and Initial Validation Studies of Anatomical Structure Morphing. , 2005, 2005, 3276-9.		0
417	A comparison study assessing the feasibility of ultrasound-initialized deformable bone models. Computer Aided Surgery, 2005, 10, 293-299.	1.8	9
418	Corpus Callosum Subdivision Based on a Probabilistic Model of Inter-hemispheric Connectivity. Lecture Notes in Computer Science, 2005, 8, 765-772.	1.0	14
419	Automatic method to assess local CT-MR imaging registration accuracy on images of the head. American Journal of Neuroradiology, 2005, 26, 137-44.	1.2	14
420	Efficient segmentation of 3D fluoroscopic datasets from mobile C-arm. , 2004, 5370, 1667.		0
421	New method to assess the registration of CT-MR images of the head. Injury, 2004, 35, 105-112.	0.7	12
422	Boundary and medial shape analysis of the hippocampus in schizophrenia. Medical Image Analysis, 2004, 8, 197-203.	7.0	224
423	Bone morphing with statistical shape models for enhanced visualization. , 2004, 5367, 122.		19
424	Correction scheme for multiple correlated statistical tests in local shape analysis. , 2004, , .		3
425	New method to assess the registration of CT-MR images of the head. , 2004, , .		5
426	A Novel Approach to Anatomical Structure Morphing for Intraoperative Visualization. Lecture Notes in Computer Science, 2004, , 478-485.	1.0	5
427	Automatic and Robust Computation of 3D Medial Models Incorporating Object Variability. International Journal of Computer Vision, 2003, 55, 107-122.	10.9	63
428	Object models in multiscale intrinsic coordinates via m-reps. Image and Vision Computing, 2003, 21, 5-15.	2.7	9
429	Evaluation of 3D Correspondence Methods for Model Building. Lecture Notes in Computer Science, 2003, 18, 63-75.	1.0	208
430	A-Mode Ultrasound–Based Registration in Computer-Aided Surgery of the Skull. JAMA Otolaryngology, 2003, 129, 1310.	1.5	37
431	Boundary and Medial Shape Analysis of the Hippocampus in Schizophrenia. Lecture Notes in Computer Science, 2003, , 464-471.	1.0	12
432	Multisite validation of image analysis methods: assessing intra- and intersite variability. , 2002, 4684, 278.		33

#	Article	IF	CITATIONS
433	Shape versus Size: Improved Understanding of the Morphology of Brain Structures. Lecture Notes in Computer Science, 2001, , 24-32.	1.0	90